Materials Today Bio 31 (2025) 101609

Contents lists available at ScienceDirect

Materials Today Bio

journal homepage: www.journals.elsevier.com/materials-today-bio

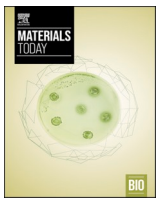

Multienzyme active melanin nanodots for antioxidant-immunomodulatory therapy of hyperoxia lung injury

Jinghua Sun [a,1], Juan Wu [a,1], Wenjing Zhao [b], Liyan Zhang [b], Yahong Han [c], Jie Dong [c], Ruiping Zhang [c,*], Yiwei Shi [a,**]

[a] NHC Key Laboratory of Pneumoconiosis, Shanxi Key Laboratory of Respiratory Diseases, Department of Pulmonary and Critical Care Medicine, The First Hospital of Shanxi Medical University, Taiyuan, China
[b] School of Pharmacy, Shanxi Medical University, Taiyuan, 030001, China
[c] The Radiology Department of Shanxi Provincial People's Hospital Affiliated to Shanxi Medical University, Taiyuan, 030001, China

ARTICLE INFO

Keywords:
Hyperoxia-induced lung injury
Melanin
Oxidative stress
Inflammation
Macrophage polarization

ABSTRACT

Supraphysiological oxygen is the most conventional method of treating patients with acute respiratory failure, but prolonged exposure to hyperoxia generates large amounts of reactive oxygen species (ROS) in the lungs, leading to hyperoxia lung injury (HLI). Nevertheless, there is no safe and effective prevention strategy. Herein, multienzyme active melanin nanodots were developed as an antioxidant-immunomodulatory defense nanoplatform for the treatment of HLI. The prepared nanodots are about 4 nm in size and are mainly composed of carbon, nitrogen and oxygen elements with high stability and multi-enzymatic activity for scavenging various reactive oxygen and reactive nitrogen radicals. Cellular experiments showed that melanin nanodots increased cell viability and ameliorated hyperoxia-induced morphological changes, mitochondrial damage and apoptosis. Meanwhile, by activating the Nrf2/Keap1/HO-1 signaling pathway, the treatment of melanin nanodots significantly inhibited the overproduction of ROS, reduced malondialdehyde, and increased the endogenous antioxidant enzyme activity in BEAS-2B cells. Interestingly, the antioxidant properties of melanin nanodots indirectly promoted the phenotypic shift of macrophages, and reduced hyperoxia-induced inflammatory responses in the damaged environment. *In vivo* NIR-II fluorescence imaging confirms the high retention of nanodots in the lungs and low accumulation in other major organs after inhalation administration, as well as the high biosafety of the melanin nanodots as they are metabolized out of the body over time via the liver and intestines. In addition, the melanin nanodots exhibited satisfactory antioxidant protection and inhibition of inflammatory cell infiltration in the lungs of HLI mouse models. Therefore, the melanin nanodots provide a potential and effective strategy for the treatment of HLI, showing great promise for application.

1. Introduction

Hyperoxia supplementation therapy gives more survival chances for severely ill and respiratory failure patients, which could effectively increase the arterial partial pressure of oxygen, further meeting the oxygen demands of tissue and organs [1,2]. However, prolonged exposure to supraphysiological concentrations of oxygen generates large amounts of reactive oxygen species (ROS) [3,4], such as highly active superoxides, hydrogen peroxide, hydroxyl radical, and other toxic products, which lead to an imbalance in the oxidative-antioxidant system in the lung, causing acute hyperoxia lung injury (HLI) [5–7]. In clinical practice, HLI occurs in 15–50 % of critically ill patients as a result of excessive oxygen therapy. Under hyperoxia conditions, excess ROS can act as direct cytotoxins causing oxidative damage to DNA, proteins, and cell membranes [8]. Moreover, these ROS can activate pro-inflammatory macrophages and release a large number of chemokines, rapidly recruiting neutrophils to migrate towards the injured lung tissues, and at the same time producing a variety of pro-inflammatory mediators like tumor necrosis factor-alpha (TNF-α), interleukin-6 (IL-6), and interleukin-1beta (IL-1β), which lead to disruption of the

* Corresponding author.
** Corresponding author.
E-mail addresses: zrp_7142@sxmu.edu.cn (R. Zhang), chinasyw225@163.com (Y. Shi).
[1] The first two authors contributed equally to this work.

https://doi.org/10.1016/j.mtbio.2025.101609
Received 16 November 2024; Received in revised form 18 February 2025; Accepted 23 February 2025
Available online 25 February 2025

alveolar-capillary barrier, increased lung permeability, massive tissue fluid infiltration, and endothelial and epithelial cell death [9,10]. In addition, the accumulation of inflammatory cells in the injured lung tissue also produces ROS, which further worsens the lung injury and even induces acute respiratory distress syndrome, which has a very high mortality rate [6,10]. Therefore, scavenging excess ROS and controlling inflammation is a promising therapeutic strategy to alleviate HLI.

Over the last few years, much attention has been devoted to examining clinical antioxidants, such as N-acetylcysteine (NAC), peroxidase, and catalase, whereas they may fail to exert satisfactory therapeutic effects for their nonspecific distribution, poor stability, low concentration at injured sites, high cost, and antigenicity [11,12]. Hence, it is necessary and urgent to develop more effective antioxidant therapeutic strategies for prevention of HLI. In recent years, nano-based antioxidants have emerged as a novel approach to improve bioavailability, enhance antioxidant activity, increase targeting capacity, and reduce adverse side effects in the treatment of acute lung injury [13–16]. In particular, the development of enzyme-mimicking nanomaterials (nanozymes) with broad-spectrum ROS scavenging capacity, robust anti-inflammatory action, easy production, and good biocompatibility is a promising strategy for treating acute injury [17–22]. Advances in nanozymes also provide new strategies for treating acute lung injury. For example, Li et al. loaded Cu nanoparticles of 2.9 nm in size onto hollow MnO_2 with the mesoporous structure to form an apoptotic cell membrane-coated antioxidant nanozyme with strong ROS scavenging ability for treating lipopolysaccharide-induced acute lung injury [23]. Yan et al. developed molybdenum nanodots with ultrasmall size and good ROS scavenging activity to protect lung tissues from acute lung injury by inhibiting the activation of the Nod-like receptor protein 3-dependent pyroptotic pathway [11]. Liu et al. reported a fluorescence carbon dot with high superoxide dismutase-like activity, which not only provided information on its biodistribution *in vivo* through fluorescence imaging, but also ameliorated acute lung injury by eliminating ROS and decreasing the levels of pro-inflammatory factors [12]. Although some therapeutic results have been achieved, most of these nanozymes are inorganic/metal-based nanomaterials, and their biodegradability and biosafety are major barriers to clinical translation [24]. Alternatively, polymer nanomaterials with ROS-scavenging capacity have been developed to alleviate oxidative stress, however, they consume ROS while degrading themselves [25]. Therefore, the exploration of polymer-based nanozymes with good biosafety and strong antioxidant capacity is beneficial in overcoming the limitations of inorganic/metal nanozymes as well as polymers with simple ROS-scavenging.

Melanin, a heterogeneous biological polymer, is a ubiquitous natural pigment present in most living organisms including humans. Recently, melanin has received widespread attention owing to its multiple advantages including natural biocompatibility and biodegradability, strong chelating capability to metal ions, and high near-infrared absorbance [26,27]. More importantly, melanin has been shown to have broad-spectrum antioxidant activity due to its multiple reductive functional groups, such as catechol, amine, and imine [28], which has been widely applied to oxidative stress-related diseases, such as kidney injury [29–31], myocardial injury [32,33], inflammatory bowel disease [34], and acute liver injury [35]. Due to the special anatomy and immune environment of the lungs, it is crucial to develop nanomaterials with multiple enzymatic activities that are more biologically safe, have smaller particle sizes, and are more stable *in vivo*. Herein, we developed melanin nanodots with multiple ROS scavenging activity and for the first time revealed their antioxidant-immunomodulatory therapy for lung injury induced by hyperoxia exposure (Fig. 1), which has not yet been demonstrated to the best of our knowledge. The results of both *in vitro and in vivo* experiments revealed that melanin nanodots could effectively relieve oxidative stress by scavenging ROS, activating the Nrf2/Keap1 signaling pathway, and promoting phenotypic shift of macrophage,

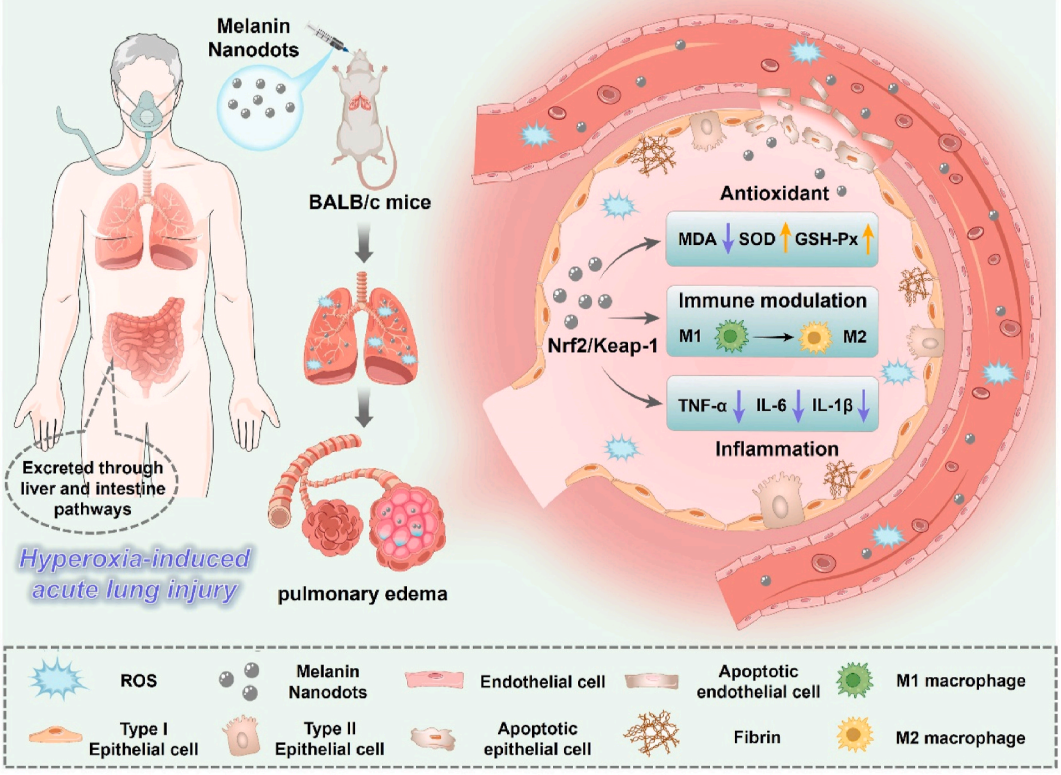

Fig. 1. Schematic illustration for the therapeutic process and mechanism of multienzyme active melanin nanodots for the treatment of HLI after intratracheal administration. The melanin nanodots effectively alleviated oxidative stress, inflammation, and lung damage by synergistic actions of broad-spectrum ROS scavenging and immune modulation of macrophage polarization. Meanwhile, the melanin nanodots could be eliminated through liver and intestine channels with minimal damage to body tissues.

subsequently inhibiting inflammatory responses in hyperoxia-induced damaged environments. Notedly, NIR-II fluorescence imaging indicated that the melanin nanodots with a size of about 4 nm could be eliminated from the body through liver and intestine pathways after intratracheal administration. We believe the biosafety and therapeutic effect of melanin nanodots as well as the therapeutic mechanism will provide a promising candidate for treating HLI.

2. Materials and methods

2.1. Materials

Melanin was acquired from Sigma-Aldrich. Sodium hydroxide (NaOH) and hydrochloric acid (37 wt% HCl) were purchased from Sinopharm Chemical Reagent Beijing Co., Ltd (Beijing, China). Amine-PEG_{5000}-amine (NH_2-PEG_{5000}-NH_2, 5 kDa), ROS detection kit (H2DCFDA) and mitochondrial membrane potential detection Kit (JC-1) were obtained from Beijing Solarbio Science & Technology Co., Ltd (Beijing, China). 2,2'-azino-bis (3-ethylbenzothiazoline 6-sulfonate) radicals (ABTS) and 2,2-Diphenyl-1-picrylhydrazyl (DPPH) were acquired from Shanghai Beyotime Biotechnology (Shanghai, China). 3-(4,5-dimethyl-2-thiazolyl)-2,5-diphenyltetrazolium bromide (MTT) and dihydroethidium (DHE) were purchased from Sigma Chemical Corporation (St. Louis, MO, USA). Apoptosis detection kit was obtained from BD Biosciences (San Jose, CA, USA). TRIzol reagent was acquired from Invitrogen (Carlsbad, CA, USA). RT reagent Kit and SYBR Green PCR Master Mix were from Promega (Madison, WI, USA). The assay kits of $O_2^{\bullet-}$, H_2O_2, OH·, malondialdehyde (MDA), superoxide dismutase (SOD), glutathione peroxidase (GSH-Px), and wright-giemsa stain were purchased from Nanjing Jiancheng Bioengineering Institute (Nanjing, China). The primary antibodies against Nrf2, Keap1, HO-1, IκBα, p-IκBα, and β-actin (1:1000) were purchased from the Cell Signaling Technology Co., Ltd (Danvers, MA, USA). The APC/Cyanine7 anti-mouse F4/80 antibody, PE anti-mouse CD86 antibody, and APC anti-mouse CD206 antibody were purchased from BioLegend Technology Co., Ltd (Beijing, China). All reagents and solvents were commercially available and used without further purification.

2.2. Preparation and characterization of melanin nanodots

Melanin nanodots were prepared according to the previous work with some modifications [36]. Briefly, pristine melanin granule (10 mg) was dissolved in NaOH aqueous solution (0.1 M) under vigorous stirring for complete dissolution, and then the right dose of HCl aqueous solution (0.1 M) was dropped to the above solution to adjust the pH to neutral. Subsequently, the neutralized solution was centrifuged and washed three times, and the melanin nanodots were obtained by freeze-drying.

The morphology of melanin nanodots was characterized by transmission electron microscopy (TEM, JEOL, Japan). The average hydrodynamic diameters and zeta potential were analyzed using a dynamic light scattering instrument (DLS, Malvern, UK). Water solubility and physiological stability of melanin nanodots in different media (PBS, DMEM, and FBS) were investigated by photography. The composition of the melanin nanodots was investigated by X-ray photoelectron spectroscopy (XPS, Kratos AXIS ULTRA DLD, Japan). Melanin nanodots solutions (12.5, 25, 50, and 100 μg/mL) were mixed with the application solution according to the instructions of the representative ROS species (e.g., $O_2^{\bullet-}$, H_2O_2, OH·, and ABTS) assay kits for evaluating multienzyme activity. The reactive nitrogen species-scavenging activity of melanin nanodots with the same gradient concentrations was tested by the DPPH assay.

2.3. Cell culture and animals

Human bronchial epithelial cells (BEAS-2B) and mouse leukemia cells of monocyte-macrophage (RAW264.7 cells) were purchased from the Cell Bank of the Chinese Academy of Sciences (Kunming, China). BEAS-2B cells were cultured in a dedicated culture media and RAW264.7 cells were grown in a DMEM high medium with conventional addition of 10 % FBS and 1 % penicillin-streptomycin.

Female BALB/c mice (6–8 weeks) were acquired from the experimental animal center of Shanxi Medical University. All animal experiments were conducted according to the institutional guidelines of Shanxi Medical University and were approved by the Institutional Animal Experiment Committee (Approval No. 2022-025, Taiyuan, China).

2.4. Cell viability assay

Cell viability was detected by MTT assay. The BEAS-2B cells were seeded (10000 cells/well) in 96-well plate overnight and incubated with different concentrations of melanin nanodots (up to 160 μg/mL) at 37 °C for 24 h. After adding MTT reagent and incubating with the cells for 20 min, cell viability was assessed using a microplate reader at 490 nm. To induce a hyperoxia cell model, the BEAS-2B cells were exposed to 90 % O_2 and 5 % CO_2 for 24 h and treated with various concentrations of melanin nanodots (0, 5, 10, 20, 40, and 80 μg/mL) for 2 h, 4 h, and 6 h. Finally, the cell viability was calculated by MTT assay.

2.5. Determination of intracellular ROS level

The fluorescence probe DCFH-DA was used to monitor the intracellular ROS level. BEAS-2B cells were seeded in a 6-well plate (3×10^5 cells/well) overnight and then were exposed to 90 % oxygen in the incubator. The cells were treated with different concentrations of melanin nanodots (0, 5, 20, and 80 μg/mL) for 6 h. After incubation with the DCFH-DA (10 μM) for 30 min, cells in each well were rinsed with PBS before adding DAPI to stain the nuclei. Finally, stained cells were imaged by a fluorescence microscope. The morphology of BEAS-2B cells before and after hyperoxia induction and nanodot treatment was observed by microscopy.

2.6. Mitochondrial membrane potential analysis

BEAS-2B cells were seeded in 6-well plate (3×10^5 cells/well) one day in advance. After exposed to 90 % O_2 and 5 % CO_2 for 24 h, the BEAS-2B cells were treated with various concentrations of melanin nanodots (5, 20, and 80 μg/mL) for 6 h. Subsequently, cells were collected, washed with PBS, and incubated with JC-1 dye for 30 min. Ultimately, cell fluorescence was determined by flow cytometer (BD LSRFortessa).

2.7. Cell apoptosis assay

BEAS-2B cells were seeded onto 6-well plate (4×10^5 cells/well) and cultured overnight. After exposed to 90 % O_2 and 5 % CO_2 for 24 h, the BEAS-2B cells were treated with various concentrations of melanin nanodots (5, 20, and 80 μg/mL) for 6 h. Then, the cells were collected and suspended in 500 μL PBS. Apoptotic cells were rapidly analyzed by flow cytometry after propidium iodide/annexin V-FITC staining.

2.8. Immunomodulatory assay in vitro

RAW264.7 cells were seeded in 6 well plates (5×10^5 cells/well) and exposed to 90 % oxygen for 24 h. Then, the cells were treated with different concentrations of melanin nanodots (5, 20, and 80 μg/mL) for 6 h. For exploring the macrophage phenotypes after melanin nanodot formulation treatment, cells were stained with anti-mouse F4/80, anti-mouse CD86, and anti-mouse CD206 for 30 min. Subsequently, the above cells were washed with PBS for three times and collected in 500 μL PBS for flow cytometry analysis (Beckman, Navios, United States).

2.9. Hyperoxia-induced mice model and nanodots treatment

The BALB/c mice were randomly divided into four groups (n = 8): (1) Control group (50 μL, Saline), (2) Hyperoxia-induced group (50 μL, Saline), (3) Hyperoxia-induced + melanin nanodots group (1 mg/mL, 50 μL), and (4) Hyperoxia-induced + NAC group (1 g/kg). The mice were exposed to 90 % O_2 in a sealed plexiglass chamber for 72 h and treated intratracheally with melanin nanodots or normal saline with the same administration or intraperitoneally injected with NAC. The different therapeutic agents were injected at 2 h before modelling and at 24 h and 48 h after modelling for 3 days. Finally, the mice were euthanatized after 72 h to collect bronchoalveolar lavage fluid (BALF) and lung tissues for further analysis. During the experiment, mice were allowed food and water ad libitum, with a 12 h day/12 h night cycle.

2.10. Measurement of cell counts and protein concentration in BALF

BALF experiment was performed on the left lung, while right lungs were harvested and preserved at −80 °C for further analysis. After centrifugation, the supernatants were preserved at −80 °C, and the cell pellets were suspended in PBS for cell counting though Wright-Giemsa staining with a hemocytometer. The protein concentrations in BALF were determined by the BCA protein assay kit (Seven, Beijing, China).

2.11. Pulmonary histopathological and immunomodulatory assay in vivo

Lung tissues were fixed in 4 % paraformaldehyde and embedded in paraffin, then cut into 5 μm slices for Hematoxylin & eosin (H&E) staining. The lung myeloperoxidase (MPO) levels were determined using immunohistochemistry staining. DHE and immunomodulatory assay were performed by immunofluorescence staining. Frozen fresh lung tissue was cut into sections of 8 μm thickness and stained with DHE. The primary (anti-mouse F4/80, anti-mouse CD86, anti-mouse CD206) antibodies, and secondary antibodies, the nuclei were labelled with DAPI. Finally, the sections were observed using fluorescence microscopy.

2.12. Measurement of biomarkers in BEAS-2B cells, BALF, and lung homogenates

Lung wet/dry ratio indicates the ratio of fresh lung tissue to dried lung tissue. The contents of oxidative products MDA, SOD, and GSH-Px in BEAS-2B cells and lung homogenates were detected using the relevant kits (Nanjing Jiancheng, China). Cell culture medium supernatant and BALF were used for the analyses of tumor necrosis factor-alpha (TNF-α), interleukin-1beta (IL-1β), and interleukin-6 (IL-6) by ELISA kits (Cloud-Clone, Wuhan, China).

2.13. Western blot analysis and quantitative real-time PCR

Cells or lung tissues were lysed by RIPA buffer. Total protein was quantified by BCA method. Protein samples were resolved by electrophoresis in 10 % SDS-PAGE gel and transferred to polyvinylidene difluoride membranes. After blocking by 5 % skimmed milk for 1 h, the membranes were incubated with anti-Nrf2 (1:1000), anti-Keap1 (1:1000), anti-HO-1 (1:1000), anti-IκBα (1:1000), anti-p-IκBα (1:1000), and β-actin (1:1000) antibodies at 4 °C overnight. After further incubation with secondary antibody for 2 h and washing, proteins were visualized with Odyssey (Licor, USA). The quantitative analysis was performed using the Image J software (National Institute of Mental Health, Bethesda, MD, USA).

Total RNA in the lung tissue was extracted and reverse-transcribed using Prime Script RT Reagent Kit (Madison, WI, USA). The obtained cDNA was then amplified with SYBR® Premix ExTaqTM Kit (Madison, WI, USA) with primer pairs specific to each gene: IL-6-Forward Primer: CCTGAACCTTC-CAAAGATGGC, IL-6-Reverse Primer: TTCACCAGGCAAGTCTCCTCA, IL-1β-Forward Primer: ATGATGGCTT-ATTACAGTGGCAA, IL-1β-Reverse Primer: GTCGGAGATTCGTAGCTGGA, TNF-α-Forward Primer: GAGGC-CAAGCCCTGGTATG, TNF-α-Reverse Primer: CGGGCCGATTGATCT-CAGC, Bcl-2-Forward Primer: GTCGCTACCGTCGTGAC.

-TTC, Bcl-2-Reverse Primer: CAGACATGCACCTACCCAGC, Bax-Forward Primer: TGAAGACAGGGGCCTTTTTG, Bax-Reverse Primer: AATTCGCCGGAGACAC-

TCG, GAPDH-Forward Primer: AGGTCGGTGTGAACGGATTTG, and GAPDH- Reverse Primer: GGGGTCGTTGATGGCAACA. Results were normalized against the RNA level of β-actin (as internal control).

2.14. Bio-distribution of fluorescence dye-labelled melanin nanodots in normal and HLI mice

Small molecular fluorescence dye IR-1061-NHS was successfully labelled on the surface of melanin nanodots. Briefly, melanin nanodots (1 mg/mL) were modified with NH_2-PEG_{5000}-NH_2 molecules at the pH = 9.5. After vigorous stirring overnight, the mixed solution was centrifuged and washed several times with deionized water to remove the free molecules. Then IR-1061-NHS was added to the PEGylated melanin nanodot solution and stirred for 2 h. After washing and centrifugation two times, near-infrared-II (NIR-II) fluorescence labelled nanodots were obtained for further application.

Healthy and hyperoxia-induced model mice (n = 4) were pretreated by intratracheal instillation of NIR-II fluorescence dye 1061-labelled nanodots. At the selected time point after administration, the mice were anesthetized and imaged by the small animal living imaging system (Suzhou Yingrui Optical Technology Co., Ltd). Furthermore, the vital organs were immediately collected and *ex vivo* imaged at 0.5, 3, 6, 12, 24, 36, 48, and 120 h after post-administration.

2.15. Biosafety evaluation in vivo

To assess the *in vivo* biosafety of melanin nanodots, healthy mice (n = 4) were injected intratracheally with PBS (50 μL) and a high dose of melanin nanodots (2 mg/mL, 50 μL) and euthanized at 2 days and 10 days. Blood cells were detected for routine blood tests. The serum was harvested to evaluate liver and kidney function, including serum alanine aminotransferase (ALT), aspartate aminotransferase (AST), urea nitrogen (BUN), and creatinine (Cre). Major organs, including heart, liver, spleen, lung, and kidneys, were collected for H&E staining analysis.

2.16. Statistical analyses

All the statistical analysis was conducted using Graph Pad Prism 9.0 and the data is expressed as mean ± standard deviation (SD). One-way analysis of variance (ANOVA) was performed. *P* values less than 0.05 were considered statistically significant. Ns represents no significant difference, * represents $P < 0.05$, ** represents $P < 0.01$, and *** represents $P < 0.001$.

3. Results and discussion

3.1. Preparation and characterization of melanin nanodots

In this study, homogeneous and water-soluble melanin nanodots were fabricated using an ultrasonication procedure [29,37]. Representative TEM image is shown in Fig. 2a. It could be observed well dispersion and uniform morphology with a size of about 4.2 nm. The as-prepared nanodots were easily dispersed in an aqueous solution (Fig. S1a) and maintained superior stability with no precipitation or residue observed in different biological media (PBS, DMEM, and FBS) for 7 days (Fig. S1b). The average dynamic size measured by DLS was about 4.9 nm (Fig. S1c), which is similar to that measured by TEM. The zeta potential of nanodots was −36.5 mV (Fig. S1d). The full spectrum survey of XPS showed three major components, C, N, and O from the melanin nanodots (Fig. S1e). The C 1s spectrum could be deconvoluted

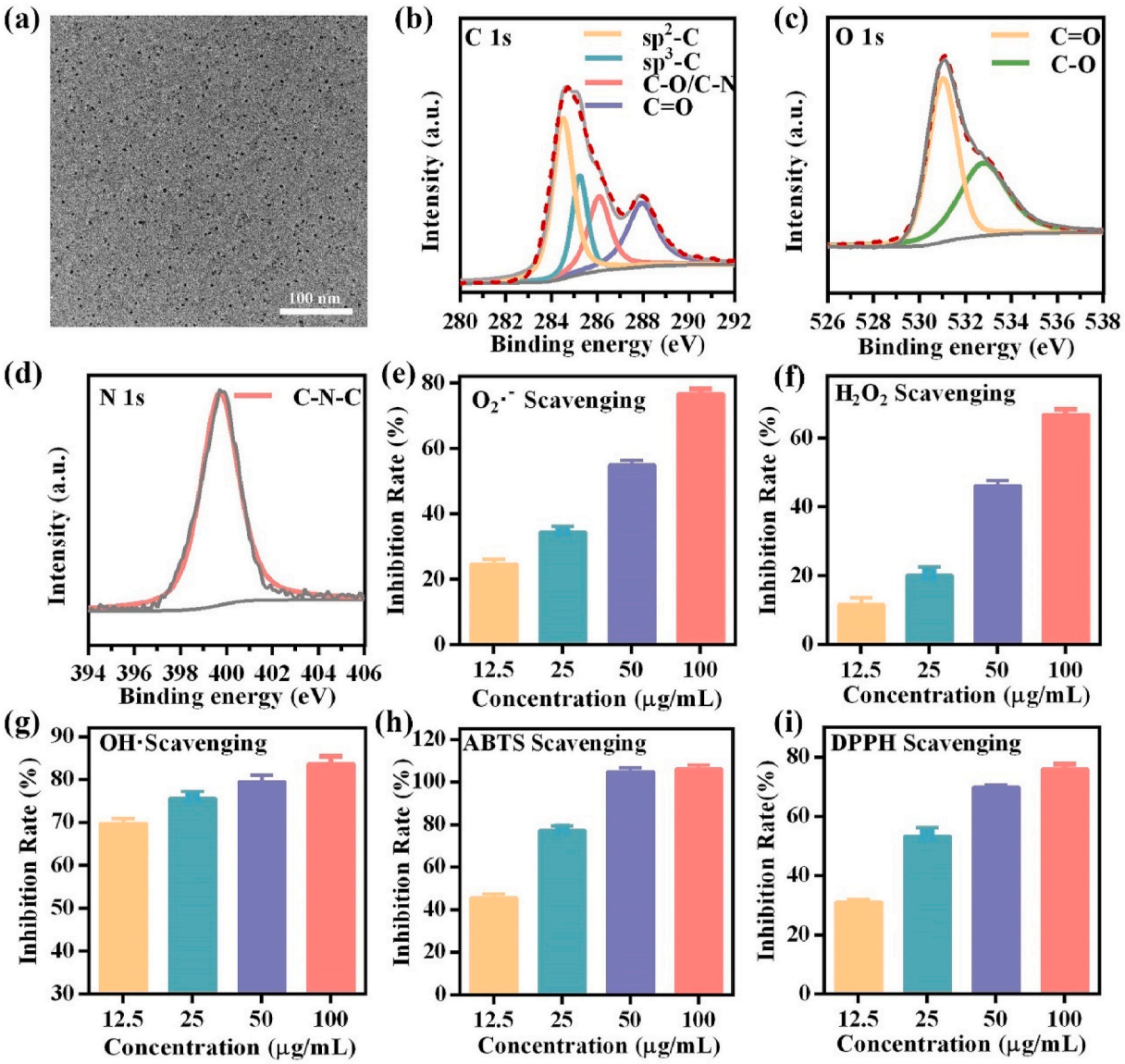

Fig. 2. Characterizations of melanin nanodots. (a) Representative TEM image of melanin nanodots. Scale bar, 100 nm. XPS spectra of C 1s (b), O 1s (C), and N 1s (d) of melanin nanodots, respectively. $O_2^{\bullet-}$ (e), H_2O_2 (f), •OH (g), ABTS (h), and DPPH (i) scavenging activity of melanin nanodots at different concentrations. Quantitative data are expressed as the means ± SD (n = 4).

into four main components including C-C (sp^2-C peak at 284.5 eV and sp^3-C peak at 285.2 eV), C-O/C-N (peak at 286.1 eV), and C=O (peak at 288 eV) (Fig. 2b) [38]. Accordingly, the O 1s spectrum could also be deconvoluted into two binding energies at 531 eV and 532.8 eV, which can be assigned to C-O and C=O (Fig. 2c). Notably, the C-N-C at 399.8 eV was observed in the peak of N 1s, demonstrating the existence of pyridinic N (Fig. 2d) [39]. Given the natural antioxidant properties of melanin, the *in vitro* ROS scavenging activity of the nanodots was evaluated at different concentrations. As depicted in Fig. 2e–g, the nanodots exhibited excellent scavenging ability for $O_2^{\bullet-}$, H_2O_2, and OH· in a concentration-dependent manner. About 76.7 ± 1.5 % of $O_2^{\bullet-}$, 66.9 ± 1.6 % of H_2O_2 and 83.6 ± 1.8 % OH· were eliminated at a concentration of 100 μg/mL, indicating the robust scavenging ability of melanin nanodots. ABTS assay and DPPH assay, which are considered universal methods for the biomaterial's antioxidant capacity, were used to assess the total antioxidant activity and reactive nitrogen radical scavenging capacity of melanin nanodots. More than 90 % ABTS· was eliminated when the nanodots concentration was 50 μg/mL (Fig. 2h) and 2i showed a good concentration dependence of melanin nanodots on DPPH clearance, further confirming that the nanodots had excellent antioxidant activity. To sum up, these results proved that the melanin nanodots had a highly efficient and broad-spectrum ROS scavenging capacity, which laid a foundation for subsequent experiments on hyperoxia-induced lung injury *in vivo*.

3.2. *In vitro cytotoxicity, cytoprotective, and immunomodulatory effects of melanin nanodots*

Encouraged by the broad-spectrum ROS scavenging activity of melanin nanodots, we next constructed cellular hyperoxia models and investigated whether they could exert a cytoprotective effect on BEAS-2B cells exposed to 90 % O_2 for 24 h (Fig. 3a). First, we assessed the cytotoxicity of melanin nanodots using the standard MTT assay. As shown in Fig. 3b, incubating BEAS-2B cells with various concentrations (5, 10, 20, 40, 80, and 160 μg/mL) of melanin nanodots for 24 h did not significantly decrease cell viability, even at the nanodots concentration up to 160 μg/mL, indicating the low cytotoxicity and superior biocompatibility. Subsequently, BEAS-2B cells were pretreated with different concentrations of

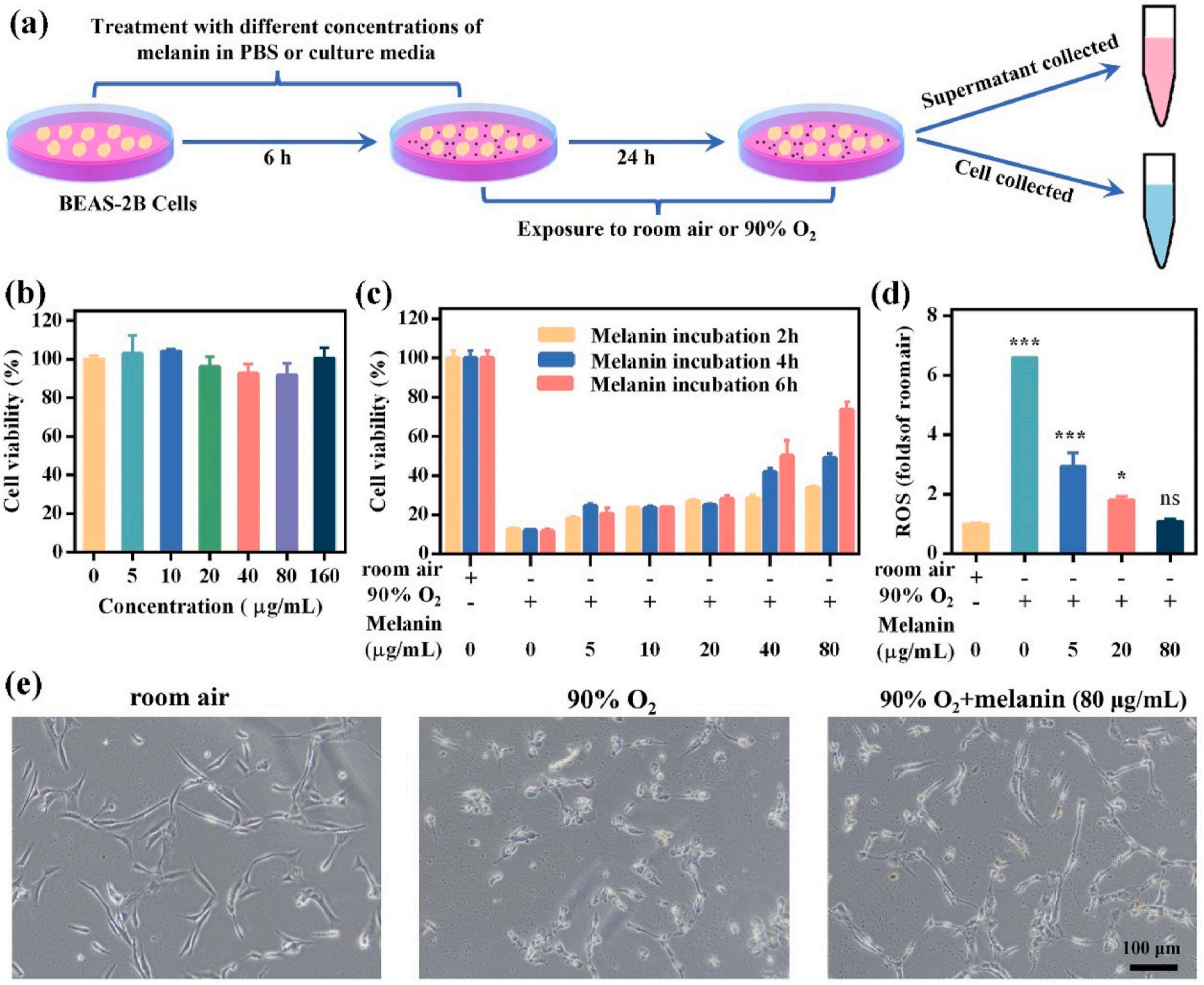

Fig. 3. The protective effects of melanin nanodots on hyperoxia-induced BEAS-2B cells *in vitro*. (a) Establishment of hyperoxia-induced BEAS-2B cells model and its treatment with different concentrations of melanin nanodots. (b) Cell viability of BEAS-2B cells incubated with different concentrations of nanodots for 24 h. (c) Cell viability of hyperoxia-induced BEAS-2B cells incubated with different concentrations of nanodots for 2, 4, and 6 h. (d) Quantitative analysis of intracellular ROS levels of hyperoxia-induced BEAS-2B cells treated with different concentrations of nanodots for 6 h. (e) Morphology analysis of normal and hyperoxia-induced BEAS-2B cells before and after treated with 80 μg/mL of melanin nanodots for 6 h, scale bar, 100 μm. Quantitative data are expressed as the means ± SD (n = 4). Significant differences (*$p < 0.01$; **$p < 0.05$; ***$p < 0.001$; and ns = no significant) compared with control group.

melanin nanodots for different periods (2, 4, and 6 h), and then exposed to 90 % O_2 for 24 h. The cell viability showed a dependence on melanin concentration and incubation time (Fig. 3c), with the highest cell viability achieved at 80 μg/mL melanin nanodots incubated with BEAS-2B cells for 6 h. Intracellular ROS levels were observed in hyperoxia-exposed BEAS-2B cells pre-treated with different concentrations of melanin nanodots using 2′,7′dichlorodihydrofluorescein diacetate (DCFH-DA) as the ROS indicator, which can convert from a non-fluorescence compound to green fluorescence 2′,7′-dichlorofluorescein upon when react with ROS [40]. DAPI was used as the nucleus indicator. As depicted in Fig. S2, intense green fluorescence signals were seen in hyperoxia-exposed cells, indicating elevated ROS levels. Nevertheless, pre-treatment of BEAS-2B cells with melanin nanodots led to a moderate reduction in ROS fluorescence signals. When the concentration of nanodots was 80 μg/mL, no remarkable green fluorescence was detected and the intensity of blue fluorescence did not change significantly, confirming the strong ROS scavenging activity of nanodots within living cells. Quantitative fluorescence intensity data presents a similar trend to the fluorescence images, and the ROS level of 80 μg/mL of melanin pre-treatment was close to that of native cells (Fig. 3d). To further confirm the cytoprotective effect of melanin nanodots, the morphology of hyperoxia-induced BEAS-2B cells before and after nanodot pretreatment was examined and shown in Fig. 3e. Normal BEAS-2B cells have a long spindle shape, whereas hyperoxia treatment significantly disrupts the morphology of the cells. The morphology of BEAS-2B cells was significantly restored after melanin nanodot pretreatment, indicating that the nanodots had a good protective effect on the cells induced by hyperoxia.

Excessive ROS produced under hyperoxia conditions are a key cause of lung injury. Large amounts of ROS in cells attack mitochondria, causing a decrease in mitochondrial membrane potential (MMP), which triggers apoptosis [41,42]. Therefore, the effect of melanin nanodots on hyperoxia-induced mitochondrial dysfunction and apoptosis was evaluated. It was found that MMP was reduced in 24 h hyperoxia-treated cells, and melanin nanodots significantly inhibited the formation of JC-1 monomers in hyperoxia-induced BEAS-2B cells. Better inhibitory effects were obtained with increasing concentrations of nanodots (Fig. 4a). It is well known that decreased MMP is a hallmark of early cell apoptosis. The percentage of apoptosis cells increased to 28.59 % after exposure to hyperoxia as compared to the apoptosis rate of 8.91 % in the control group (Fig. 4b). It was found that the percentage of apoptotic cells decreased gradually with increasing concentration of melanin nanodots. 80 μg/mL of melanin nanodots significantly inhibited hyperoxia-induced apoptosis of BEAS-2B cells. These results suggest that melanin nanodot pretreatment significantly reverses hyperoxia-induced MMP changes and apoptosis in BEAS-2B cells.

Macrophages are the first responders to injury and one of the crucial

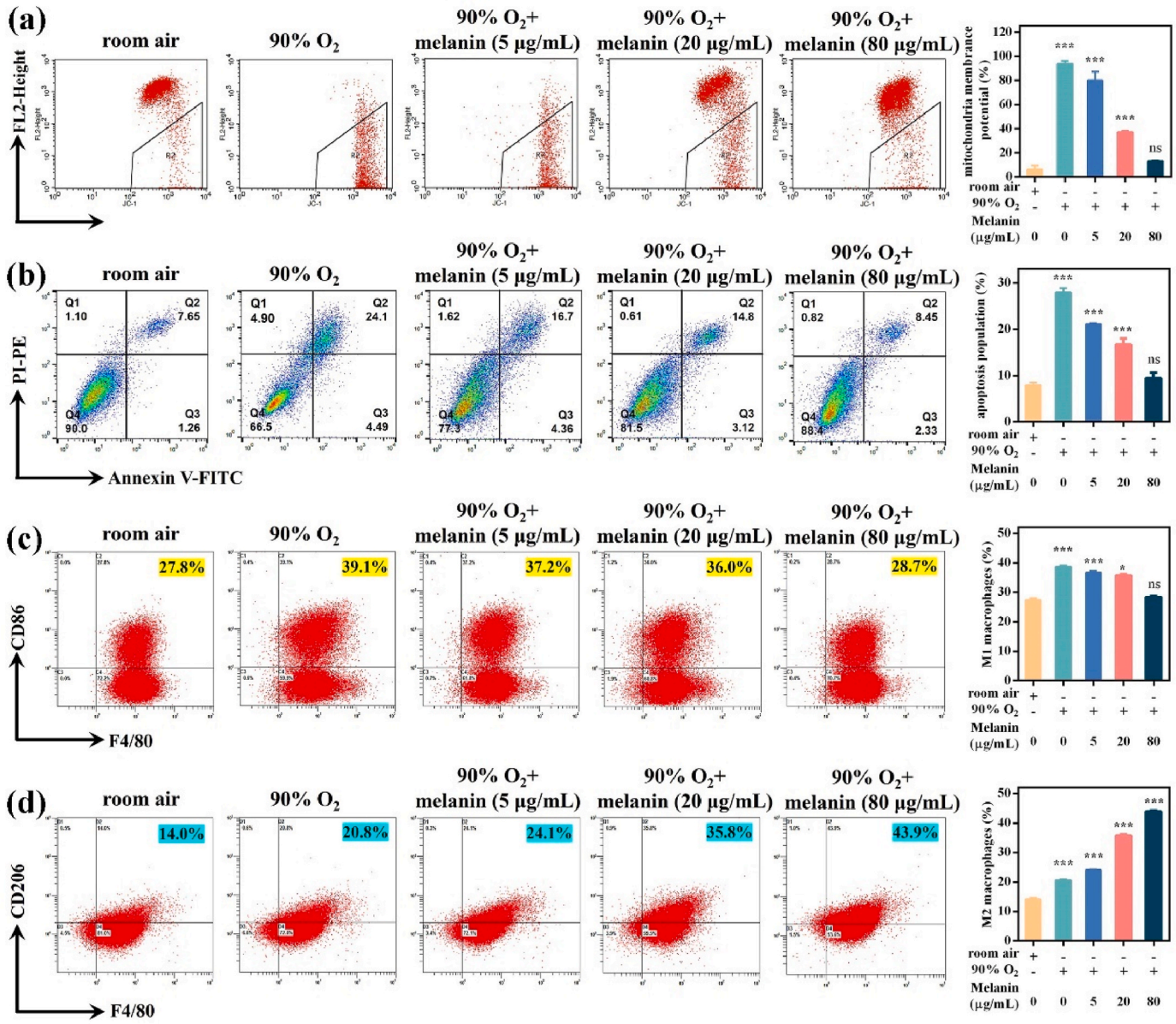

Fig. 4. The antioxidant, anti-apoptotic and immunomodulatory activities of melanin nanodots on hyperoxia-induced BEAS-2B cells *in vitro*. (a) Flow cytometry and corresponding quantitative analysis of MMP in hyperoxia-induced BEAS-2B cells treated with different concentrations of melanin nanodots. (b) Flow cytometry and corresponding quantitative analysis of apoptosis distribution in hyperoxia-induced BEAS-2B cells treated with different concentrations of melanin nanodots. Representative flow cytometric analyses and quantitative data of M1 phenotype macrophages (c) and M2 phenotype macrophages (d). Quantitative data are expressed as the means ± SD (n = 4). Significant differences (*$p < 0.01$; **$p < 0.05$; ***$p < 0.001$; and ns = no significant) compared with control group.

of components the natural immune system. In the inflammatory microenvironment, macrophages are known for their polarization behaviors toward the proinflammatory (M1 phenotype macrophages) and anti-inflammatory (M2 phenotype macrophages) phenotype. M1 phenotype macrophages release abundant proinflammatory mediators and chemokines that recruit neutrophils and monocytes, while M2 phenotype macrophages promote tissue repair by accelerating inflammation resolution [15,43]. Here, the influence of melanin nanodots on immunomodulatory therapy was analyzed by flow cytometry. Normally, we utilized $F4/80^+CD86^+$ to label M1 phenotype macrophages (Fig. 4c) and $F4/80^+CD206^+$ to label M2 phenotype macrophages (Fig. 4d). As shown in Fig. 4c and d, hyperoxia exposure significantly increased the level of CD86 in macrophages (39.1 %) from 27.8 % of untreated RAW 264.7 cells, and the level of CD206 in macrophages also increased (20.8 %), as compared to that the group with untreated macrophages (14.0 %), indicating the M1 phenotypic activation of RAW 264.7 cells because of the secret of excess proinflammatory mediators with a lot of ROS generation. As the concentration of co-incubated melanin nanodots increased, the level of CD86 gradually decreased. When incubated with 80 μg/mL melanin nanodots, the number of M1-type macrophages was significantly reduced to 28.7 %, which is close to normal. In contrast, population expression of M2 phenotypic macrophages continued to be upregulated until 43.9 %. Therefore, melanin nanodots played a significant role in exerting the immunomodulatory effect by promoting the transition of RAW 264.7 cells from the M1 phenotype to the M2 phenotype, thereby effectively inhibiting hyperoxia-induced lung injury.

3.3. In vitro cytoprotective mechanism of melanin nanodots

It is generally believed that hyperoxia-induced lung injury produces a large number of ROS, leading to the development of lipid peroxidation [9]. MDA is one of the products formed by the reaction between lipids and oxygen free radicals, which represents the degree of lipid peroxidation [44]. On the contrary, SOD and GSH-Px could alleviate the damage caused by oxidative stress [45]. As shown in Fig. 5a–c, after hyperoxia exposure, MDA levels in the cells increased dramatically, while SOD and GSH-Px activities were significantly reduced. Excitingly, pretreatment with different concentrations of melanin nanodots resulted in a significant fall in MDA levels and a distinct increase in SOD and GSH-Px levels, all in a concentration-dependent manner. When the concentration of melanin nanodots was 80 μg/mL, the activities of these three factors almost returned to normal levels. These results suggest that melanin nanodot pretreatment successfully reduced the level of oxidative stress in BEAS-2B cells under hyperoxia exposure.

To unravel the molecular mechanisms by which melanin nanodots alleviate hyperoxia-induced oxidative stress in cells, we assessed changes in key signaling molecules in the ROS regulatory network. It is known that the nuclear factor-related factor 2 (Nrf2) Kelch-like ECh-associated protein 1 (Keap1) signaling pathway is involved in various types of oxidative damage [46,47]. Nrf2 is a key regulator of the endogenous antioxidant response, and Nrf2-activated release of Keap1 is a key negative regulator that induces the expression of many antioxidant genes. Evidence has shown that Nrf2 activation induces the expression of multiple classical antioxidant genes and enhances survival in lung injury models of hyperoxia exposure [48,49]. Some studies have confirmed that induction of Nrf2 is an important strategy to relieve oxidative stress [50]. Except for those two factors, heme oxygenase 1 (HO-1) is also one of the antioxidant genes and can reduce the production of intracellular ROS [51]. Although the Nrf2/Keap1 signaling

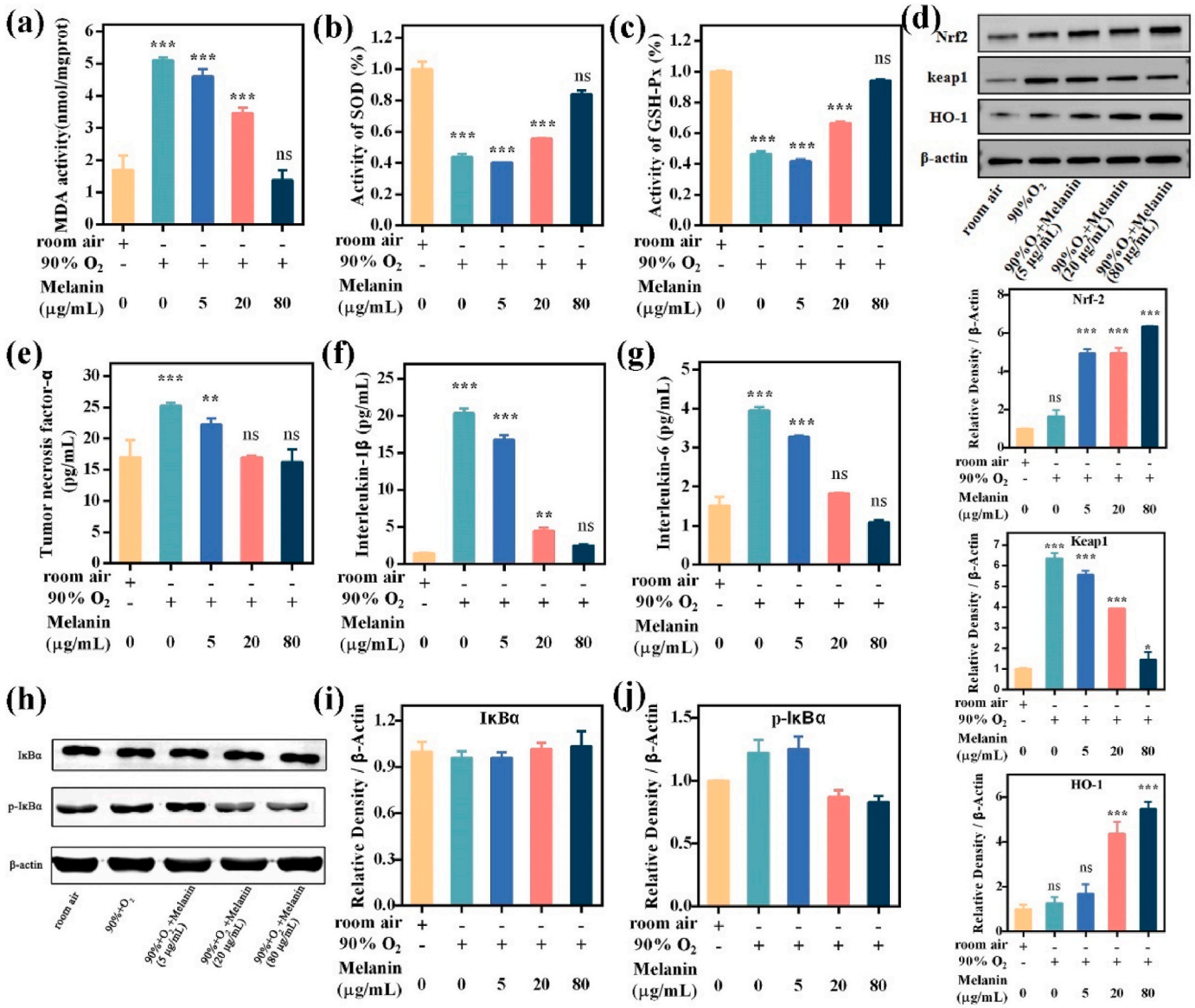

Fig. 5. Cytokine levels and molecular mechanisms of melanin nanodot therapy. The levels of MDA (a), SOD (b), and GSH-Px (c) in hyperoxia-induced BEAS-2B cells treated with different concentrations of melanin nanodots. (d) The expression of Nrf2, Keap-1, and HO-1 in hyperoxia-induced BEAS-2B cells under various treatments were evaluated by western blot analysis. Changes in the levels of representative inflammatory factors TNF-α (e), IL-1β (f), and IL-6 (g) in hyperoxia-induced BEAS-2B cells under different treatments. (h) The expression of p-IκBα and IκBα in hyperoxia-induced BEAS-2B cells under different treatments were evaluated by western blot assay. Quantitative data are expressed as the means ± SD (n = 4). Significant differences (*$p < 0.01$; **$p < 0.05$; ***$p < 0.001$; and ns = no significant) compared with control group.

pathway plays an important role in the regulation of oxidative stress, it is unclear whether it is involved in the changes of hyperoxia injury intervened by melanin nanodots. For this reason, we used Western blot analysis to examine the levels of Nrf2 and its associated proteins (HO-1 and Keap1). As shown in Fig. 5d, the results revealed that the expression of Nrf2 and HO-1 slightly increased, while the main repressor targeted Keap1 markedly increased after hyperoxia treatment. Interestingly, the expressions of Nrf2 and HO-1 were significantly increased and the expression of Keap1 was reduced by the treatment of melanin nanodots. It was speculated that the melanin nanodots inhibited hyperoxia-induced oxidative stress in a dose-dependent manner, which may be associated with the upregulation of the Nrf2/Keap1 pathway.

Considering that hyperoxia-induced lung injury is usually accompanied by an inflammatory response, then the effects of melanin nanodots on the expression of pro-inflammatory cytokines and inflammation-related proteins were explored. The levels of pro-inflammatory cytokines were significantly increased in the hyperoxia group. On the contrary, the contents of TNF-α (Fig. 5e), IL-1β (Fig. 5f), and IL-6 (Fig. 5g) decreased in a dose-dependent manner with the increase of melanin nanodots, reflecting that the nanodots could reduce the rise of hyperoxia-induced inflammatory factors. Since the suppressive effects of nanodots on inflammation usually depend on the downregulation of proinflammatory signaling, we focused on the role of the nuclear factor kappa B (NF-κB) signaling pathway. The suppressor protein (IκB) is an important member of the NF-κB signaling pathway, regulating the activation and transcription of NF-κB. As shown in Fig. 5h–j, the expression of p-IκBα was slightly increased, while the expression of IκBα was slightly decreased in the hyperoxia group compared with the control group. After melanin treatment, the expressions of p-IκBα and IκBα were both slightly changed, which was inconsistent with the changes of nanodots to pro-inflammatory cytokines. From the above results, we can speculate that melanin nanodots alleviate oxidative stress and inhibit inflammation mainly through antioxidant effects, which leads to the reduction of intracellular lipid peroxidation factor and inflammatory factor levels, indirectly decreasing the cellular inflammatory response, rather than directly down-regulating anti-inflammatory signaling pathways.

3.4. Biodistribution and metabolism of melanin nanodots in HLI mice models

To investigate the feasibility of melanin nanodots in the treatment of HLI *in vivo*, we first studied their biodistribution and metabolism in hyperoxia-induced mice models. Mice were endotracheally injected with IR-1061-labelled melanin nanodots and subsequently established the model of HLI by hyperoxia exposure, and then the NIR-II fluorescence imaging was performed to track the distribution of melanin nanodots at designated time points. As depicted in Fig. 6a and b, compared to the un-injected mice, a significant fluorescence signal appeared in the lung at 0.5 h after injection, indicating that the nanodots had successfully entered the lungs. Meanwhile, there was a slight enhancement of the fluorescence signal with time extension until 12 h due to the diffusion of melanin nanodots in lung tissue. Subsequently, the fluorescence signals in the lungs weakened, and obvious fluorescence signals appeared in the liver, spleen, and intestine at 24 h. The results showed that a large number of melanin nanodots in the lungs were metabolized by the liver and intestines and excreted from the body at 24 h, suggesting that our optimal dosing time is 24 h. With the prolongation of time, the fluorescence signals of each organ in the mice weakened or even disappeared. After 120 h of melanin nanodot injection, only weak fluorescence signals were observed in the lungs, indicating that most of the melanin nanodots had been metabolized and excreted from the body. In addition, we used non-hyperoxia-exposed mice as a control to study the metabolic behavior of melanin nanodots in mice under normal and hyperoxia conditions (Fig. S3). After intratracheal injection of melanin nanodots in mice in the non-hyperoxia-exposed group, the fluorescence signals in the lungs of mice were first enhanced and then gradually weakened with the extension of time, showing a similar trend of change as that of the hyperoxia group. Differently, in the non-hyperoxia group, strong fluorescence signals were observed in the liver and intestine 6 h after injection and negligible fluorescence signals were observed in the lungs after 48 h, while in the hyperoxia-exposed group, fluorescence signals were observed in the liver and intestine only at 24 h and weak fluorescence signals were still detected in the lungs at 120 h after injection. The results showed that melanin nanodots were metabolized faster in normal mice with shorter retention time in the lungs, whereas they showed high accumulation and retention in the lungs of the hyperoxia group, which was mainly attributed to the destruction of endothelial structure of the pulmonary vasculature and the increase in permeability due to the complex microenvironment under hyperoxia, which led to the passive retention of the nanodots [16].

Fluorescence images and intensity quantification of isolated major organs in the HLI mouse model were shown in Fig. 6c–e. In all isolated tissues, the fluorescence signal is barely detectable in the heart, kidneys, muscles, and blood, whereas significant fluorescence signals were detected in the liver, spleen, and intestine, and peaked at 24 h and then decreased to near normal values over time. The results show that a large number of melanin nanodots are mainly excreted through hepatic and intestinal metabolism, which further ensures their biosafety *in vivo*. NIR-II fluorescence imaging results show that melanin nanodots can reach the lungs and achieve prolonged retention, facilitating timely clearance of ROS to play a role. Moreover, these ultra-small-sized nanodots can penetrate the barrier to enter the liver and intestinal system for excretion from the body without metastatic deposition in the lungs, ensuring better biosafety. In addition, the *in vivo* distribution revealed by NIR-II imaging also helped us to determine the optimal dosing time to enhance the precision of treatment.

3.5. Therapeutic effect of melanin nanodots in HLI mice

Inspired by strong ROS scavenging ability *in vitro* and NIR-II fluorescence imaging results, we investigated the therapeutic efficacy of melanin nanodots in the HLI mice model. At 2 h pre-hyperoxia stimulation, melanin nanodots were given to mice for the first time. During the process of treatment, nanodots were given every 24 h. At 72 h post-endotracheal administration, BALF and lung tissues in each group were carefully collected for further analysis (Fig. 7a). The clinical manifestations of HLI are mainly the influx of protein-rich oedema fluid into the alveoli due to impaired capillary endothelium-alveolar epithelial barrier and increased permeability [52]. To determine whether melanin nanodots could alleviate the HLI, the microscopic features of the lung tissue were compared among the control group, hyperoxia-exposed group, melanin-treated group, and NAC-treated group. As depicted in the representative H&E images of Fig. 7b, the control mice had normal lung histology and no pathological changes were observed. Hyperoxia exposure caused pulmonary histopathological changes, including that the alveolar space was ruptured, red blood cells were noticeably observed in some alveolar spaces, and inflammatory cell infiltration was observed. There was a slight alleviation in the lung tissue of NAC-treated mice. In contrast, hyperoxia-induced lung inflammation and oedema were significantly suppressed after melanin nanodots were administered during continuous inhalation of highly concentrated oxygen. The dry-to-wet (W/D) ratio of the lungs is crucial in determining the severity of pulmonary oedema [53]. In this experiment, the highest dry-to-wet ratio was found in the hyperoxia-exposed group, indicating severe pulmonary oedema (Fig. 7c). NAC could reduce the severity of pulmonary oedema to some extent. However, injection of melanin nanodots dramatically reduced hyperoxia-induced pulmonary oedema. Inspired by these data, we further measured protein concentrations and identified different infiltrating cells in BALF. The protein concentrations and total cell counts in BALF were highly increased in mice with hyperoxia

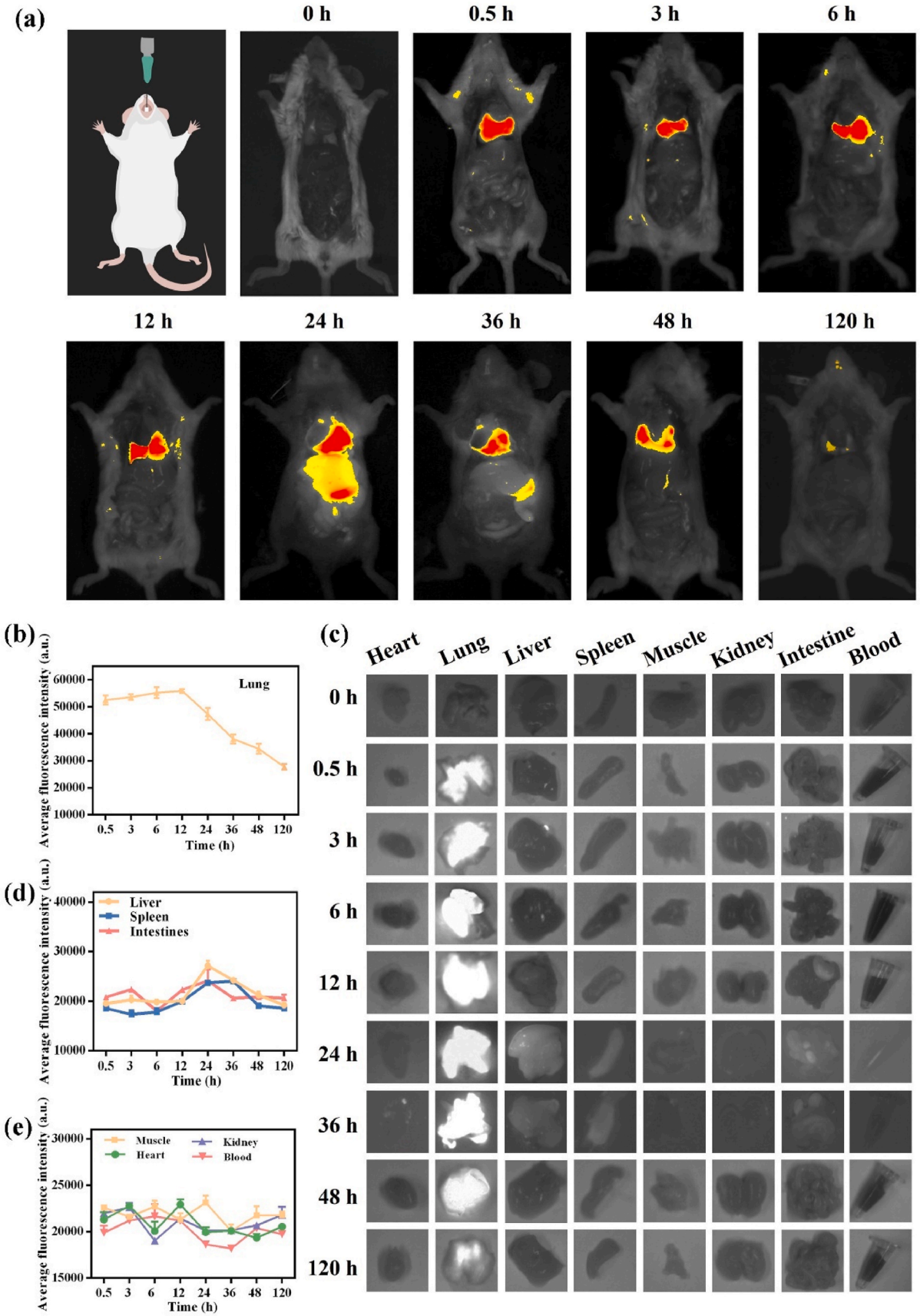

Fig. 6. Biodistribution and clearance efficiency of melanin nanodots *in vivo*. (a) NIR-II fluorescence images of hyperoxia-induced mice after being treated with IR-1061-labelled melanin nanodots at predetermined time points. (b) Quantitative fluorescence intensity of lung tissues at selected time points. (c) Fluorescence images of main organs *ex vivo*. (d) Quantitative fluorescence intensity of live, spleen, and intestines. (e) Quantitative fluorescence intensity of muscle, kidney, heart, and blood at selected time points. Quantitative data are expressed as the means ± SD (n = 4).

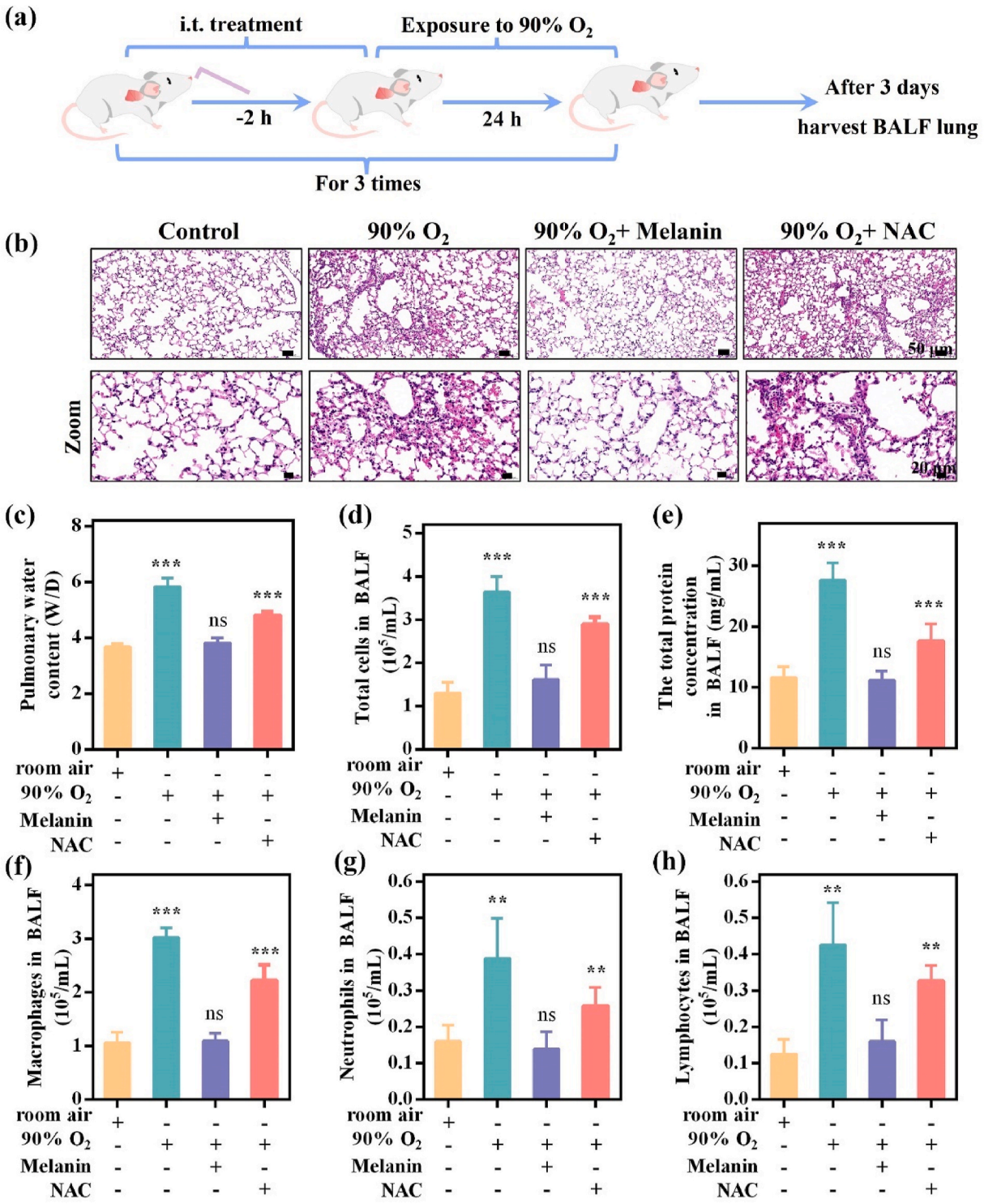

Fig. 7. *In vivo* therapeutic efficacy of melanin nanodots on HLI mice. (a) Establishment of the HLI model and experimental schedule of HLI mice treated with melanin nanodots. (b) H&E staining images of lung tissues treated with saline, melanin nanodots, and NAC. Scale bars are 50 μm and 20 μm for the overview and magnified images, respectively. (c) The wet/dry (W/D) ratios of lung tissues treated with saline, melanin nanodots, and NAC. The levels of total cell (d), total protein (e), macrophages (f), neutrophils (g), and lymphocytes (h) in BALF under different treatments. Quantitative data are expressed as the means ± SD (n = 6). Significant differences (**$p < 0.05$; ***$p < 0.001$; and ns = no significant) compared with control group.

exposure (Fig. 7d and e). Following the therapy with NAC, there was some decrease in the protein concentrations and total cell counts. As expected, pre-treated with melanin nanodots significantly relieved the hyperoxia-induced elevation of BALF total cell counts. Then, we analyzed the sub-populations of the infiltrated cells in BALF. After the treatment of melanin, the number of macrophages (Fig. 7f), neutrophils (Fig. 7g), and lymphocytes (Fig. 7h) decreased significantly as compared with other groups, demonstrating that melanin nanodots pretreatment suppressed inflammatory cell infiltration in the lung of HLI.

Then, the analysis of lung homogenate was used to reveal important antioxidant protective effects of melanin nanodots on hyperoxia-induced mice. Fig. 8a–c shows the changes in oxidative stress

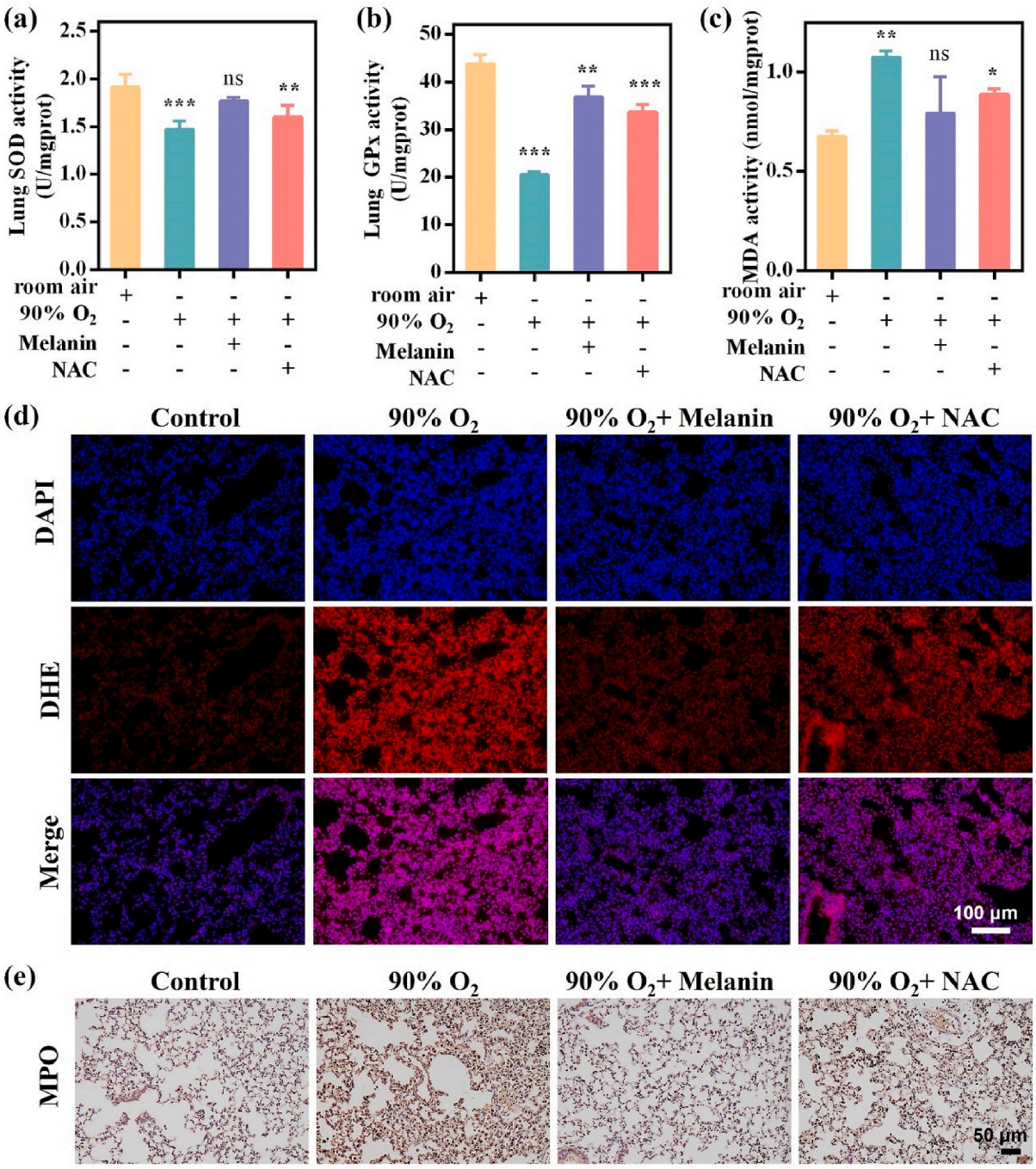

Fig. 8. Melanin nanodots suppressed oxidative damage and ROS level in HLI mice. The levels of MDA (a), SOD (b), and GSH-Px (c) in lung homogenates of different treatment groups. (d) Dihydroethidium (DHE) stained images of lung tissues harvested from different treatment groups. Blue fluorescence represents nuclei (DAPI) and red fluorescence represents ROS (DHE). Scale bar, 100 μm. (e) Immunohistochemical staining (MPO) of lung tissues in different treatment groups. Brown areas represent MPO-positive cells. Scale bar, 50 μm. Quantitative data are expressed as the means ± SD (n = 6). Significant differences (*$p < 0.01$; **$p < 0.05$; ***$p < 0.001$; and ns = no significant) compared with control group. (For interpretation of the references to colour in this figure legend, the reader is referred to the Web version of this article.)

parameters (MDA) and antioxidant enzyme levels (SOD and GSH-Px) in lung tissues, respectively. Among them, MDA levels were significantly higher in the hyperoxia group, indicating that lipid peroxidation occurred in lung tissue after hyperoxia induction. The MDA level evidently decreased after melanin nanodot treatment (Fig. 8a). The NAC had some effectiveness as well, although not as much as the nanodots. Meanwhile, it was also observed that the levels of antioxidant enzymes (SOD and GSH-Px) in lung tissues were both significantly decreased by hyperoxia exposure (Fig. 8b and c), whereas SOD and GSH-Px activities were restored to normal range after melanin nanodot treatment. Free NAC group remains less effective than melanin nanodot-treated group. We further assessed ROS levels in the lung tissue of mice by dihydroethidium (DHE) staining (Fig. 8d and Fig. S5a) [40,54]. Compared with the normal group, ROS production was significantly increased in the lung tissues of mice in the hyperoxia-exposed group, and after treatment with melanin nanodots, the bright red fluorescence was dramatically attenuated, indicating a significant decrease in the level of ROS, which reconfirmed the powerful ROS-scavenging ability of

melanin nanodots. Bright red fluorescence still appeared in the NAC group, indicating that a certain amount of ROS still existed, mainly due to the faster metabolism of small molecule drugs and the short retention time at the site of lung injury, thus limiting the efficacy. Myeloperoxidase (MPO) is also a unique marker associated with oxidative stress that catalyzes the production of reactive oxygen intermediates [11]. Excessive MPO was observed in lung tissues after hyperoxia exposure as shown in Fig. 8e. Treatment with NAC resulted in a moderate decrease in MPO levels. MPO expression was significantly reduced in the nanodot-treated group, which had a distinct effect. All these results revealed that the melanin nanodots could effectively inhibit oxidative stress in HLI model.

Pro-inflammatory cytokines are strongly associated with HLI development and progression [55]. Fig. 9a–c presented the change in expression levels of representative inflammatory factors including IL-1β, IL-6, and TNF-α in the BALF of the HLI mouse model. The expression levels of these inflammatory factors in BALF were considerably higher in the hyperoxia group compared to the control group. After treatment with NAC, small reductions were observed in the levels of these inflammatory factors. Surprisingly, the expression of these pro-inflammatory cytokines in nanodots-treated group decreased significantly and almost returned to normal levels. Interestingly, the mRNA levels of IL-1β (Fig. S4a), IL-6 (Fig. S4b), and TNF-α (Fig. S4c) in the lung tissue exhibited similar trends to those in the BALF. As a result, melanin nanodots significantly inhibit the expression of inflammatory cytokines and reverse the lung inflammatory environmental imbalance under hyperoxia exposure.

Next, we evaluated the levels of M1 and M2 macrophages in the lung tissue by immunofluorescence staining. Immunostaining images demonstrated that lung tissues from hyperoxia-induced mice displayed high expression levels of the M1 macrophage marker CD86 (Fig. 8d and Fig. S5b) and low expression levels of the M2 macrophage marker CD206 (Fig. 8e and Fig. S5c), suggesting the presence of a pro-inflammatory lung microenvironment. Interestingly, melanin nanodot treatment increased the number of CD206-labelled M2-type macrophages, and reduced the number of CD86-labelled M1-type macrophages, compared with saline and NAC groups. This finding reaffirms that melanin nanodots can reverse the inflammatory immune microenvironment by promoting a shift from the M1 macrophage to the M2 phenotype, which is consistent with our cellular-level observations. In addition, we examined the expression levels of Nrf2/Keap1/HO-1 in lung tissues of mice (Fig. 9f). Compared with the normal group, Keap-1 protein expression was increased and Nrf2 and HO-1 were not significantly altered in lung tissues of mice in the hyperoxia-exposed group. After different treatments, free NAC slightly decreased Keap-1 expression and elevated Nrf2 and HO-1 expression. In contrast, melanin nanodots had the strongest ability to inhibit Keap-1 expression and substantially elevate Nrf2 and HO-1 expression.

Hyperoxia supplementation therapy provides a greater chance of survival for critically ill patients and those with respiratory failure by providing adequate oxygen to organs and tissues in the short term. However, prolonged exposure to oxygen above physiological concentrations can lead to HLI and ultimately to acute respiratory distress syndrome, which has a high fatality rate. However, there are no effective treatments available. Small molecule drugs with antioxidant and anti-inflammatory effects have not achieved the expected therapeutic effects in clinical trials. Here, NAC was chosen as a positive drug and its therapeutic effect on HLI was investigated. The results showed that NAC had some alleviating effect on HLI, but the efficacy was limited, which is consistent with the results reported in the literature [11,53,56]. The main reason is that, on the one hand, NAC has limited ability to scavenge free radicals, especially for the superoxide anions that are abundant in lung tissue after HLI occurs, it has almost no scavenging effect [53,57]. On the other hand, NAC is a small molecule drug with a short half-life and low bioavailability. The rapid development of nanomedicines in recent years has brought new hope for HLI treatment. However, the potential biosafety of nanomaterials, complex synthesis processes, and unclear *in vivo* therapeutic mechanisms limit their clinical translation. Melanin nanodots in this work not only have ultra-small size, good water solubility and high environmental stability, but also have strong scavenging ability for a variety of free radicals. *In vivo and in vitro* results showed that melanin nanodots could regulate the Nrf2/Keap1/HO-1 signaling pathway by scavenging reactive free radicals to significantly alleviate oxidative damage, inhibit apoptosis, and reverse macrophage polarization to reduce inflammation. In addition, melanin nanodots can be retained for a long period of time in the lung tissue of hyperoxia-induced mice and subsequently metabolized out of the body. Hematology and histology also demonstrated the high biosafety of the nanodots. Therefore, melanin nanodots can be used as a potential agent for the treatment of HLI and show promising clinical applications.

3.6. *In vivo biosafety of melanin nanodots*

Lastly, the *in vivo* biosafety of high-dose melanin nanodots was evaluated. As shown in Fig. S6a, the routine blood results of mice in both PBS and melanin nanodot groups reached normal levels at 2 and 10 days after intratracheal injection. Furthermore, representative biomarkers of liver and kidney function, such as ALT, AST, BUN, and Cre were assessed. There were no significant differences in these biomarkers between mice treated with PBS and those receiving the melanin nanodots at 2 or 10 days. Additionally, H&E staining of the heart, liver, spleen, lung, and kidney of mice also showed no visible damage (Fig. S6b). These results demonstrated that melanin nanodots exhibited good biosafety even at high injection doses in mice.

4. Conclusion

In summary, we have successfully prepared the melanin nanodots for the treatment of hyperoxia-induced lung injury, which possess potent antioxidant, anti-inflammatory, and immunoregulation abilities. These ultra-small nanodots are not only easy to synthesize, highly water-soluble and stable, but also scavenge a wide range of free radicals ($O_2^{\bullet -}$, H_2O_2, •OH, ABTS, and DPPH). *In vitro* cellular experiments revealed that melanin nanodots had negligible cytotoxicity, effectively scavenging intracellular ROS and protecting cell morphology. Moreover, the nanodots treatment significantly restored mitochondrial membrane potential, inhibited apoptosis and reversed macrophage polarization, thereby effectively reducing oxidative and inflammatory factor levels (MDA, IL-1β, IL-6, and TNF-α). *In vivo* imaging results demonstrated that melanin nanodots could remain in lung tissue for 24 h after endotracheal injection, and can be completely metabolized and excreted with time, without producing metastatic deposits in the lung, which is highly biosafe. In a hyperoxia-exposed mouse model, melanin nanodot treatment significantly reduced lung inflammation and oedema, alleviated lung histological changes, inhibited oxidative damage and reduced ROS levels compared to saline and NAC-treated groups. More importantly, both *in vivo* and *in vitro* experiments confirmed that melanin nanodots exert therapeutic effects by modulating the Nrf2/Keap1/HO-1 signaling pathway. Therefore, our findings will provide a new promising strategy for the efficient treatment of HLI and further facilitate its clinical application in future biomedical treatments and research.

CRediT authorship contribution statement

Jinghua Sun: Writing – original draft, Validation, Methodology, Investigation. **Juan Wu:** Validation, Methodology, Investigation. **Wenjing Zhao:** Validation, Investigation, Data curation. **Liyan Zhang:** Project administration, Data curation. **Yahong Han:** Supervision, Project administration. **Jie Dong:** Resources, Data curation. **Ruiping Zhang:** Writing – review & editing, Funding acquisition, Data curation, Conceptualization. **Yiwei Shi:** Validation, Investigation.

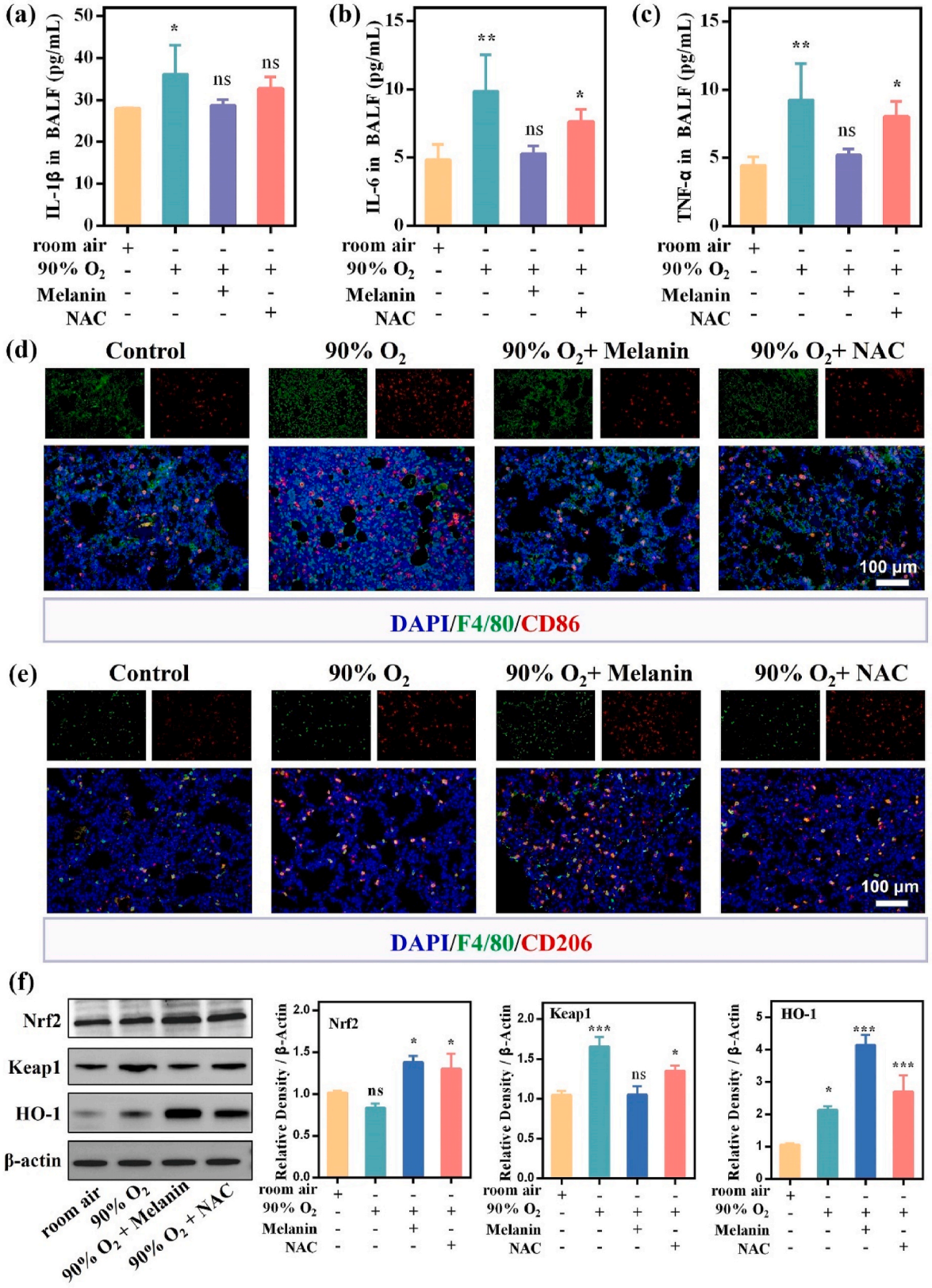

Fig. 9. The levels of IL-1β (a), IL-6 (b), and TNF-α (c) in BALF under different treatments. (d, e) Immunofluorescence images of the lung tissues stained with F4/80 (green), CD86 (M1 marker, red), and CD206 (M2 marker, red). The nuclei of lung tissues were stained by DAPI. Scale bar, 100 μm. (f) The expression of Nrf2, Keap-1, and HO-1 in the lung tissues under different treatments were evaluated by western blot analysis. Quantitative data are expressed as the means ± SD (n = 6). Significant differences (*$p < 0.01$; **$p < 0.05$; ***$p < 0.001$; and ns = no significant) compared with control group. (For interpretation of the references to colour in this figure legend, the reader is referred to the Web version of this article.)

Declaration of competing interest

We declare that we do not have any commercial or associative interest that represents a conflict of interest in connection with the work submitted.

Acknowledgments

This work has been financially supported by the National Natural Science Foundation of China (No. 32271429, 82071987, and 82120108016), the National Key R&D Program of China (No. 2023YFC3402800), China Postdoctoral Science Foundation (No. 2022M722002), Natural Science Research Project of Shanxi Province (No. 202203021211243), and Key Laboratory of Nano-imaging and Drug-loaded Preparation of Shanxi Province (No. 202104010910010).

Appendix A. Supplementary data

Supplementary data to this article can be found online at https://doi.org/10.1016/j.mtbio.2025.101609.

Data availability

Data will be made available on request.

References

[1] C.Y. Hong, H.D. Zhang, X.Y. Liu, Y. Xu, Attenuation of hyperoxic acute lung injury by Lycium barbarum polysaccharide via inhibiting NLRP3 inflammasome, Arch Pharm. Res. (Seoul) 42 (2019) 902–908.
[2] O.D. Saugstad, Oxygen and oxidative stress in bronchopulmonary dysplasia, J. Perinat. Med. 38 (2010) 571–577.
[3] S. Chen, Q. Wu, D. Zhong, C. Li, L. Du, Caffeine prevents hyperoxia-induced lung injury in neonatal mice through NLRP3 inflammasome and NF-κB pathway, Respir. Res. 21 (2020) 140.
[4] M. Zhao, S. Tang, J. Xin, Y. Wei, D. Liu, Reactive oxygen species induce injury of the intestinal epithelium during hyperoxia, Int. J. Mol. Med. 41 (2018) 322–330.
[5] J. Wang, A. Zhang, Y. Li, J. Xu, F. Huang, M. Zhao, B. Wu, S. He, Effect of intermittent hypoxia or hyperoxia on lung development in preterm rat neonates during constant oxygen therapy, J. Cell. Biochem. 120 (2019) 17545–17554.
[6] K. Fukuhara, T. Nakashima, M. Abe, T. Masuda, H. Hamada, H. Iwamoto, K. Fujitaka, N. Kohno, N. Hattori, Suplatast tosilate protects the lung against hyperoxic lung injury by scavenging hydroxyl radicals, Free Radic. Biol. Med. 106 (2017) 1–9.
[7] D. Zheng, D. Liu, Y. Kuang, J. Xu, G. Xu, Q. Tai, Toll-like receptor 7 deficiency mitigates hyperoxia-induced acute lung injury in mice, Biomed. Pharmacother. 129 (2020) 110345.
[8] S.P. Reddy, P.M. Hassoun, R. Brower, Redox imbalance and ventilator-induced lung injury, Antioxidants Redox Signal. 9 (2007) 2003–2012.
[9] R. Alva, M. Mirza, A. Baiton, L. Lazuran, L. Samokysh, A. Bobinski, C. Cowan, A. Jaimon, D. Obioru, T. Al Makhoul, J.A. Stuart, Oxygen toxicity: cellular mechanisms in normobaric hyperoxia, Cell Biol. Toxicol. 39 (2022) 111–143.
[10] F. Dias-Freitas, C. Metelo-Coimbra, R. Roncon-Albuquerque Jr., Molecular mechanisms underlying hyperoxia acute lung injury, Respir. Med. 119 (2016) 23–28.
[11] J. Yan, Z. Tang, Y. Li, H. Wang, J.C. Hsu, M. Shi, Z. Fu, X. Ji, W. Cai, D. Ni, J. Qu, Molybdenum nanodots for acute lung injury therapy, ACS Nano 17 (2023) 23872–23888.
[12] C. Liu, W. Fan, W.X. Cheng, Y. Gu, Y. Chen, W. Zhou, X.F. Yu, M. Chen, M. Zhu, K. Fan, Q.Y. Luo, Red emissive carbon dot superoxide dismutase nanozyme for bioimaging and ameliorating acute lung injury, Adv. Funct. Mater. 33 (2023) 2213856.
[13] A. Garcia-Fernandez, F. Sancenon, R. Martinez-Manez, Mesoporous silica nanoparticles for pulmonary drug delivery, Adv. Drug Deliv. Rev. 177 (2021) 113953.
[14] J. Li, L. Chen, C. Li, Y. Fan, M. Zhan, H. Sun, S. Mignani, J.P. Majoral, M. Shen, X. Shi, Phosphorus dendron nanomicelles as a platform for combination anti-inflammatory and antioxidative therapy of acute lung injury, Theranostics 12 (2022) 3407–3419.
[15] C. Huang, Q. You, J. Xu, D. Wu, H. Chen, Y. Guo, J. Xu, M. Hu, H. Qian, An mTOR siRNA-loaded spermidine/DNA tetrahedron nanoplatform with a synergistic anti-inflammatory effect on acute lung injury, Adv. Healthcare Mater. 11 (2022) e2200008.
[16] Q. Qiao, X. Liu, T. Yang, K. Cui, L. Kong, C. Yang, Z. Zhang, Nanomedicine for acute respiratory distress syndrome: the latest application, targeting strategy, and rational design,, Acta Pharm. Sin. B 11 (2021) 3060–3091.
[17] R. Yuan, Y. Li, S. Han, X. Chen, J. Chen, J. He, H. Gao, Y. Yang, S. Yang, Y. Yang, Fe-curcumin nanozyme-mediated reactive oxygen species scavenging and anti-inflammation for acute lung injury, ACS Cent. Sci. 8 (2021) 10–21.
[18] X. Duan, B. Liu, A nanozymatic solution to acute lung injury,, ACS Cent. Sci. 8 (2022) 7–9.
[19] K. Wang, Y. Zhang, W. Mao, W. Feng, S. Lu, J. Wan, X. Song, Y. Chen, B. Peng, Engineering ultrasmall ferroptosis-targeting and reactive oxygen/nitrogen species-scavenging nanozyme for alleviating acute kidney injury, Adv. Funct. Mater. 32 (2021) 2109221.
[20] H. Wu, F. Xia, L. Zhang, C. Fang, J. Lee, L. Gong, J. Gao, D. Ling, F. Li, A ROS-sensitive nanozyme-augmented photoacoustic nanoprobe for early diagnosis and therapy of acute liver failure,, Adv. Mater. 34 (2022) e2108348.
[21] S. Zhang, X.-D. Zhang, Recent Advances in the bioactive structure and application of single-atom nanozymes, Nano Biomedicine and Engineering 16 (2024) 1–27.
[22] X. Song, Q. Huang, Y. Yang, L. Ma, W. Liu, C. Ou, Q. Chen, T. Zhao, Z. Xiao, M. Wang, Y. Jiang, Y. Yang, J. Zhang, Y. Nan, W. Wu, K. Ai, Efficient therapy of inflammatory bowel disease (IBD) with highly specific and durable targeted Ta2C modified with chondroitin sulfate (TACS), Adv. Mater. 35 (2023) 2301585.
[23] H. Ji, C. Zhang, F. Xu, Q. Mao, R. Xia, M. Chen, W. Wang, S. Lv, W. Li, X. Shi, Inhaled pro-efferocytic nanozymes promote resolution of acute lung injury, Adv. Sci. (2022) e2201696.
[24] A. Sahu, K. Min, S.H. Jeon, K. Kwon, G. Tae, Self-assembled hemin-conjugated heparin with dual-enzymatic cascade reaction activities for acute kidney injury, Carbohydr. Polym. 316 (2023) 121088.
[25] C. Shi, J. Dawulieti, F. Shi, C. Yang, Q. Qin, T. Shi, L. Wang, H. Hu, M. Sun, L. Ren, F. Chen, Y. Zhao, F. Liu, M. Li, L. Mu, D. Liu, D. Shao, K.W. Leong, J. She, A nanoparticulate dual scavenger for targeted therapy of inflammatory bowel disease,, Sci. Adv. 8 (2022) eabj2372.
[26] H. Liu, Y. Yang, Y. Liu, J. Pan, J. Wang, F. Man, W. Zhang, G. Liu, Melanin-like nanomaterials for advanced biomedical applications: a versatile platform with extraordinary promise,, Adv. Sci. 7 (2020) 1903129.
[27] J. Sun, Y. Han, J. Dong, S. Lv, R. Zhang, Melanin/melanin-like nanoparticles: as a naturally active platform for imaging-guided disease therapy, Materials Today Bio 23 (2023) 100894.
[28] Y. Liu, K. Ai, X. Ji, D. Askhatova, R. Du, L. Lu, J. Shi, Comprehensive insights into the multi-antioxidative mechanisms of melanin nanoparticles and their application to protect brain from injury in ischemic stroke, J. Am. Chem. Soc. 139 (2017) 856–862.
[29] J. Sun, X. Zhao, H. Shen, J. Dong, S. Rong, W. Cai, R. Zhang, CD44-targeted melanin-based nanoplatform for alleviation of ischemia/reperfusion-induced acute kidney injury, J. Contr. Release 368 (2024) 1–14.
[30] J. Sun, J. Han, J. Dong, X. Zhai, R. Zhang, A kidney-targeted chitosan-melanin nanoplatform for alleviating diabetic nephropathy through modulation of blood glucose and oxidative stress,, Int. J. Biol. Macromol. 264 (2024) 130663.
[31] X. Zhao, J. Sun, J. Dong, C. Guo, W. Cai, J. Han, H. Shen, S. Lv, R. Zhang, An auto-photoacoustic melanin-based drug delivery nano-platform for self-monitoring of acute kidney injury therapy via a triple-collaborative strategy, Acta Biomater. 147 (2022) 327–341.
[32] C. Liu, Q. Zou, H. Tang, J. Liu, S. Zhang, C. Fan, J. Zhang, R. Liu, Y. Liu, R. Liu, Y. Zhao, Q. Wu, Z. Qi, Y. Shen, Melanin nanoparticles alleviate sepsis-induced myocardial injury by suppressing ferroptosis and inflammation, Bioact. Mater. 24 (2023) 313–321.
[33] J. Zhou, W. Liu, X. Zhao, Y. Xian, W. Wu, X. Zhang, N. Zhao, F.J. Xu, C. Wang, Natural melanin/alginate hydrogels achieve cardiac repair through ROS scavenging and macrophage polarization, Adv. Sci. (2021) e2100505.
[34] Y. Liu, C. Gao, G. Li, Z. Niu, X. Liu, H. Shen, J. Sun, R. Zhang, Melanin nanoparticle-modified probiotics for targeted synergistic therapy of ulcerative colitis, ACS Appl. Mater. Interfaces 16 (2024) 31950–31965.
[35] C. Zhao, Z. Li, J. Chen, L. Su, J. Wang, D.S. Chen, J. Ye, N. Liao, H. Yang, J. Song, J. Shi, Site-specific biomimicry of antioxidative melanin formation and its application for acute liver injury therapy and imaging, Adv. Mater. (2021) e2102391.
[36] J. Sun, W. Xu, L. Li, B. Fan, X. Peng, B. Qu, L. Wang, T. Li, S. Li, R. Zhang, Ultrasmall endogenous biopolymer nanoparticles for magnetic resonance/photoacoustic dual-modal imaging-guided photothermal therapy, Nanoscale 10 (2018) 10584–10595.
[37] J. Sun, W. Cai, Y. Sun, C. Guo, R. Zhang, Facile synthesis of melanin-dye nanoagent for NIR-II fluorescence/photoacoustic imaging-guided photothermal therapy, Int. J. Nanomed. 15 (2020) 10199–10213.
[38] Y. Zou, X.F. Chen, P. Yang, G.J. Liang, Y. Yang, Z.P. Gu, Y.W. Li, Regulating the absorption spectrum of polydopamine, Sci. Adv. 6 (2020) eabb4696.
[39] B.Y. Guan, S.L. Zhang, X.W. Lou, Realization of walnut-shaped particles with macro-/mesoporous open channels through pore architecture manipulation and their use in electrocatalytic oxygen reduction, Angew. Chem., Int. Ed. 57 (2018) 6176–6180.
[40] Y. Li, D. Liu, T. Chen, J. Song, X. Yu, Q. Liu, J. Qi, W. Li, Inhaled NIR-II nanocatalysts for real-time monitoring and immunomodulatory therapy of acute lung injury, Adv. Funct. Mater. (2024) 2403183.
[41] D. Zou, J. Li, Q. Fan, X. Zheng, J. Deng, S. Wang, Reactive oxygen and nitrogen species induce cell apoptosis via a mitochondria-dependent pathway in hyperoxia lung injury, J. Cell. Biochem. 120 (2018) 4837–4850.
[42] Z. Yiran, J. Chenyang, W. Jiajing, Y. Yan, G. Jianhong, B. Jianchun, L. Xuezhong, L. Zongping, Oxidative stress and mitogen-activated protein kinase pathways involved in cadmium-induced BRL 3A cell apoptosis, Oxid. Med. Cell. Longev. 2013 (2013) 516051.

[43] X. Huang, H. Xiu, S. Zhang, G. Zhang, The role of macrophages in the pathogenesis of ALI/ARDS,, Mediat. Inflamm. 2018 (2018) 1264913.
[44] Y.B. Chen, Y.B. Zhang, Y.L. Wang, P. Kaur, B.G. Yang, Y. Zhu, L. Ye, Y.L. Cui, A novel inhalable quercetin-alginate nanogel as a promising therapy for acute lung injury,, J. Nanobiotechnol. 20 (2022) 272.
[45] S. He, L. Wu, H. Sun, D. Wu, C. Wang, X. Ren, Q. Shao, P. York, J. Tong, J. Zhu, Z. Li, J. Zhang, Antioxidant biodegradable covalent cyclodextrin frameworks as particulate carriers for inhalation therapy against acute lung injury, ACS Appl. Mater. Interfaces 14 (2022) 38421–38435.
[46] P. Canning, F.J. Sorrell, A.N. Bullock, Structural basis of Keap1 interactions with Nrf2, Free Radic. Biol. Med. 88 (2015) 101–107.
[47] R. Zhao, L. Wang, T. Wang, P. Xian, H. Wang, Q. Long, Inhalation of MSC-EVs is a noninvasive strategy for ameliorating acute lung injury, J. Contr. Release 345 (2022) 214–230.
[48] A.G. Gauthier, J. Wu, M. Lin, R. Sitapara, A. Kulkarni, G.A. Thakur, E.E. Schmidt, J. C. Perron, C.R. Ashby Jr., L.L. Mantell, The positive allosteric modulation of alpha7-nicotinic cholinergic receptors by GAT107 increases bacterial lung clearance in hyperoxic mice by decreasing oxidative stress in macrophages,, Antioxidants 10 (2021) 135.
[49] G. Zheng, H. Ren, H. Li, X. Li, T. Dong, S. Xu, Y. Yan, B. Sun, J. Bai, Y. Li, Lycium barbarum polysaccharide reduces hyperoxic acute lung injury in mice through Nrf2 pathway, Biomed. Pharmacother. 111 (2019) 733–739.
[50] H.L. Zhao, S. Eguchi, A. Alam, D.Q. Ma, The role of nuclear factor-erythroid 2 related factor 2 (Nrf-2) in the protection against lung injury,, Am J Physiol-Lung C 312 (2017) L155–L162.
[51] F. Feng, P. Cheng, H. Zhang, N. Li, Y. Qi, H. Wang, Y. Wang, W. Wang, The protective role of tanshinone IIA in silicosis rat model via TGF-beta1/smad signaling suppression, NOX4 inhibition and Nrf2/ARE signaling activation,, Drug Des. Dev. Ther. 13 (2019) 4275–4290.
[52] Z. Liang, H. Yue, C. Xu, Q. Wang, S. Jin, Protectin DX relieve hyperoxia-induced lung injury by protecting pulmonary endothelial glycocalyx, J. Inflamm. Res. 16 (2023) 421–431.
[53] W. Muhammad, M. Liang, B. Wang, J. Xie, W. Ahmed, C. Gao, NAC-grafted ROS-scavenging polymer nanoparticles for modulation of acute lung injury microenvironment in vivo, Biomacromolecules 26 (2024) 528–540.
[54] J. Yan, Y. Wang, J. Zhang, X. Liu, L. Yu, Z. He, Rapidly blocking the calcium overload/ROS production feedback loop to alleviate acute kidney injury via microenvironment-responsive BAPTA-AM/BAC Co-delivery nanosystem, Small 19 (2023) e2206936.
[55] Y. Guo, Y. Liu, S. Zhao, W. Xu, Y. Li, P. Zhao, D. Wang, H. Cheng, Y. Ke, X. Zhang, Oxidative stress-induced FABP5 S-glutathionylation protects against acute lung injury by suppressing inflammation in macrophages, Nat. Commun. 12 (2021) 7094.
[56] S. Kim, S.Y. Kim, S.J. Rho, S.H. Kim, S.H. Song, C.H. Kim, H. Lee, S.K. Kim, Biocompatible N-acetyl-nanoconstruct alleviates lipopolysaccharide-induced acute lung injury in vivo, Sci. Rep. 11 (2021) 22662.
[57] S. Wu, Y. Shi, L.T. Jiang, W.Z. Bu, K. Zhang, W.Z. Lin, C. Pan, Z.B. Xu, J.W. Du, H. Chen, H.H. Wang, N-Acetylcysteine-Derived carbon dots for free radical scavenging in intervertebral disc degeneration, Adv. Healthcare Mater. 12 (2023) 2300533.